Nanoscale

Accepted Manuscript

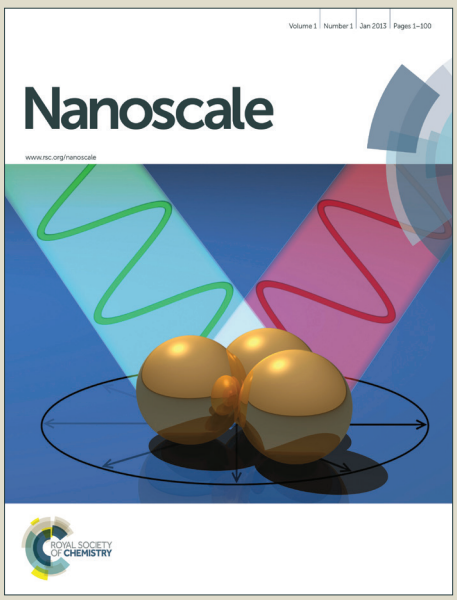

ROYAL SOCIETY OF CHEMISTRY

www.rsc.org/nanoscale

Journal Name

RSCPublishing

ARTICLE

Chirality effects at each amino acid position on tripeptide self-assembly into hydrogel biomaterials

Cite this: DOI: 10.1039/xoxxoooooox

S. Marchesan*[a,b], C. D. Easton[a], K. E. Styan[a], L. J. Waddington[a], F. Kushkaki[c], L. Goodall[a], K. M. McLean[a], J. S. Forsythe[d], and P. G. Hartley[a].

Received ooth January 2012,
Accepted ooth January 2012

DOI: 10.1039/xoxxoooooox

www.rsc.org/

Hydrogels formed by ultrashort peptides are emerging as cost-effective materials for cell culture. However, L-peptides are labile to proteases, while their D-isomers are thought to not support cell growth as well. In contrast, self-assembly behaviour and biological performance of heterochiral peptides (i.e., made of both D and L amino acids) are largely unknown. In this study, we evaluate the effects of amino acid chirality on tripeptide self-assembly and hydrogelation at physiological pH, and cytocompatibility in fibroblast cell culture. A series of uncapped hydrophobic tripeptides with all combinations of D, L amino acids was prepared, tested for self-assembly under physiological conditions, and analysed by circular dichroism, FT-IR, cryo-TEM, AFM, and Thioflavin T fluorescence imaging. Amino acid chirality has a profound effect on the peptides' supramolecular behaviour. Only selected isomers form hydrogels, and of amyloid structure, as confirmed by rheology and XRD. Importantly, they are able to maintain the viability and proliferation of fibroblasts *in vitro*. This study identifies two heterochiral gels that perform well in cell culture and will assist in the design of innovative and cost-effective peptide gel biomaterials.

Introduction

Hydrogel biomaterials, including those based on self-assembly of a range of peptides, have attracted increasing interest in the scientific community in recent years, for applications in cell culture, tissue engineering, and wound healing.[1-6] Nonetheless, we are still generally not able to design new gelling peptides – especially short ones – completely *ex novo* and to anticipate their rheological behaviour; gelling peptide sequences are usually found by serendipity or by molecular iteration around a known gelling example.[7] An understanding of the self-assembly process is thus of value for a variety of reasons. Firstly, it allows the production of adaptive materials that respond to changes in the environment, as reversible gels are able to assemble, disassemble and reassemble into macromolecular structures through non-covalent cross-links.[8-12] This is very relevant in a biological context, where cells proliferate and evolve over time. Secondly, it sheds light on the spontaneous assembly of natural proteins into complexes with acquired function, a process that regulates both physiological and pathological cellular activities.[13,14] Thirdly, it provides new tools for the design of next generation 'smart' materials, where simple building blocks self-organize in sophisticated architectures that respond to stimuli.[2, 3, 15, 16]

In particular, ultrashort peptide derivatives, which typically exploit synthetic end-caps (e.g. Naphthalene, Fmoc, etc.) to achieve gelation under physiological conditions, are attractive building blocks for cost-effective biomaterials.[17-20] Typically, a change of the solubility of the hydrogelator is used to trigger self-assembly. In particular, a popular approach relies on a pH switch, which can be induced by a number of methods.[21-23] Recently, we reported the first examples of uncapped, solvent-free, tripeptides capable of the rapid formation of self-supporting hydrogels under physiological conditions,[24, 25] with obvious advantages as biomaterial.[26, 27] These systems are simple and cheap to prepare, and readily gel upon the mixing of two precursor solutions of different pH. An intriguing feature of these particular tripeptides is the finding that, under identical

conditions, L-tripeptides do not self-assemble into persistent nanostructures, while rapid gelation is achieved upon introduction of a D-amino acid at the *N*-terminus. Thus far, we could not anticipate the supramolecular behaviour of other stereoisomers and here, to answer this question, we investigate the effects of chirality at any position in the peptide sequence on conformation, self-assembly, and cytotoxicity. Moreover, tripeptides are known to be the minimal motif required to deliver a biological signal.[28] Thus, developing an understanding of their supramolecular behaviour is of high interest to identify tripeptides that form bioactive gels, and to answer important biological questions in cell signalling.

The ability to use chirality to fine-tune self-assembly, and the interactions of the resulting gel with cells and tissues, is an interesting new concept in the field of biomaterials.[29-31] The majority of peptide hydrogel studies to date have employed homochiral molecules, with only a few exceptions[32], which is not surprising given that biomacromolecules are homochiral (e.g., L-proteins and D-sugars). An understanding of how cells interact with gels of different chirality may prove important as we seek to engineer innovative biomaterials with improved performance, and better resistance to degradation.[33, 34] In this study, we report for the first time the effects of chirality at each amino acid position in a series of hydrophobic tripeptides that exploit two phenylalanines as the self-assembling motif. Eight tripeptides were prepared with all combinations of D, L amino acids, and they were tested for their ability to undergo hydrogelation triggered by a pH change to 7.4. The eight tripeptides were assessed for their secondary conformation (using CD, FT-IR), supramolecular self-assembly (using cryo-TEM, AFM, amyloid stained fluorescence), and rheological properties. Gels were then investigated by XRD and evaluated using fibroblast cell culture to identify their suitability for the development of biomaterials that may allow probing of these important questions.

Results and Discussion

Tripeptide secondary structure.

To investigate how self-assembly is affected by changes in chirality at each position in the tripeptide sequence, we prepared a series of stereoisomers with all possible combinations of D and L amino acids (Table 1) and tested their ability to self-assemble at physiological pH. The secondary conformation of each tripeptide was assessed by CD, FT-IR, and Thioflavin T (ThT) fluorescence microscopy. In general, CD spectra of enantiomers had key features that were mirror images relative to the baseline,

No. of D amino acids	Tripeptide sequence (enantiomer pair)
0	Phe-Phe-Val (**I**)
1	^{D}Phe-Phe-Val (**II**), Phe-^{D}Phe-Val (**III**), Phe-Phe-^{D}Val (**IV**)
2	Phe-^{D}Phe-^{D}Val (**II**), ^{D}Phe-Phe-^{D}Val (**III**), ^{D}Phe-^{D}Phe-Val (**IV**)
3	^{D}Phe-^{D}Phe-^{D}Val (**I**)

Table 1. The peptide series with sequence Phe-Phe-Val includes 8 isomers with all possible combinations of D, L amino acids. Enantiomers are marked with matching symbols (i.e., **I-IV**).

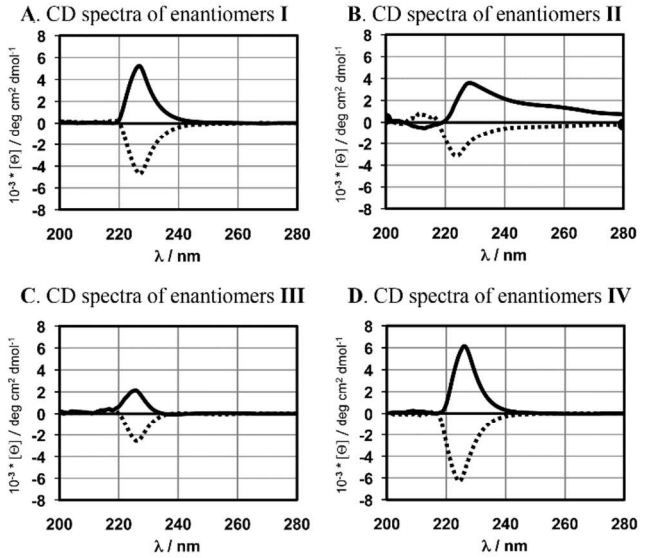

Fig. 1. CD spectra of tripeptide enantiomers **I-IV**: A) Phe-Phe-Val (black line) and ^{D}Phe-^{D}Phe-^{D}Val (dotted line); B) ^{D}Phe-Phe-Val (black line) and Phe-^{D}Phe-^{D}Val (dotted line); C) ^{D}Phe-Phe-^{D}Val (black line) and Phe-^{D}Phe-Val (dotted line); D) Phe-Phe-^{D}Val (black line) and ^{D}Phe-^{D}Phe-Val (dotted line).

as expected (Fig. 1). Every peptide spectrum was characterised by either a positive maximum or a negative minimum in the region 225-235 nm, indicative of π-π stacking of phenylalanines with either L or D chirality, respectively. In the case of peptides with aromatic residues of either configuration (i.e., LD or DL), the π-π stacking signal was weaker, and, interestingly, it was driven on either side of the baseline by the chirality of the amino acid central to the sequence (i.e., in position 2), and not the *N*-terminal. This observation is counterintuitive, considering the key role played in our systems by the *N*-terminus, where substitution of an L-amino acid (in L-tripeptides) with its D-enantiomer leads to hydrogelation.[24, 25] In addition, a recent report has described the case of dipeptide derivatives that self- assemble into nanoribbons, with handedness dictated by the chirality of the *N*-terminal amino acid.[35]

Six of the eight tripeptides did not show any unambiguous sign of predominant secondary conformation in the region 200-220 nm, as generally is the case for such short peptides. Only enantiomers **II**, i.e. ^{D}Phe-Phe-Val and Phe-^{D}Phe-^{D}Val (Fig. 1B) clearly displayed the presence of beta-sheets, with chirality driven also in this case by the central amino acid, and not the *N*-terminal (i.e., negative minimum or positive maximum in the region 210-220 nm, as expected for either L or D peptides, respectively). In addition, these two peptides differed from the other stereoisomers in the width of their π-π stacking signal, which in these two cases alone extended well beyond 240 nm. Overall, these observations indicate that intermolecular interactions are particularly sensitive to amino acid chirality at the different positions along the tripeptide, with discontinuous

chirality (i.e., DLD or LDL as in enantiomers **III**) leading to the weakest CD signal (Fig. 1C). A key role is played by the amino acid that is central to the sequence (i.e., in position 2) as it drives

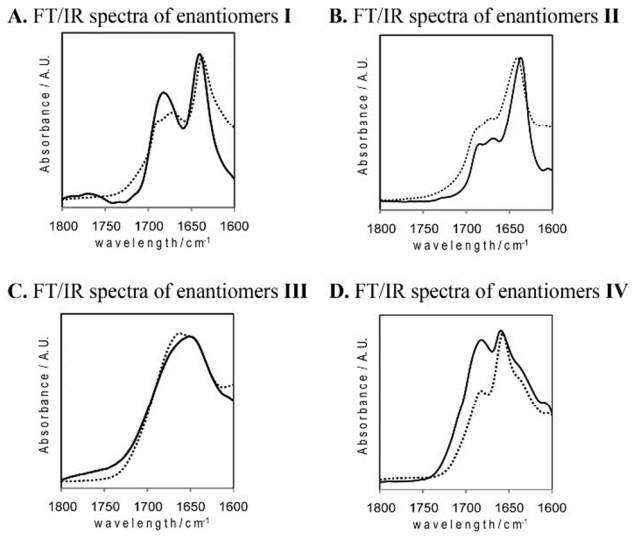

Fig. 2. FT-IR spectra of tripeptide enantiomers **I-IV**: A) Phe-Phe-Val (black line) and ^{D}Phe-^{D}Phe-^{D}Val (dotted line); B) ^{D}Phe-Phe-Val (black line) and Phe-^{D}Phe-^{D}Val (dotted line); C) ^{D}Phe-Phe-^{D}Val (black line) and Phe-^{D}Phe-Val (dotted line); D) Phe-Phe-^{D}Val (black line) and ^{D}Phe-^{D}Phe-Val (dotted line).

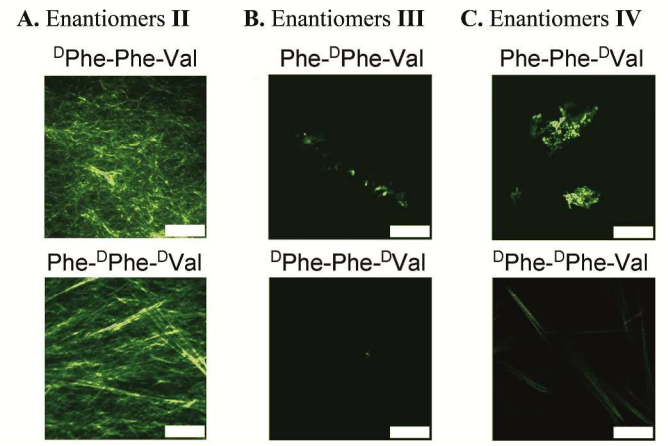

Fig. 3. Thioflavin T (ThT) fluorescence microscopy reveals structures with extended beta-sheet conformation for six of the eight tripeptides. Enantiomers **II** (A) are the only ones that form a network of self-assembled fibers that extend over several microns in length; in contrast, only isolated structures are seen for enantiomers **III** (B) and **IV** (C). Scale bar = 10 microns.

the chirality of the CD signal (i.e., above or below the baseline) for both the π-π stacking and the beta-sheets that may be present.

To better assess secondary structures, tripeptides were also analysed by FT-IR (Fig. 2) and ThT fluorescence microscopy (Fig. 3), which highlights the presence of structures with extended beta-sheet conformation.[36] Analogous to CD, FT-IR spectra of the amide region of enantiomers are similar, with minor differences that could be attributed to traces of trifluoroacetic acid (responsible for the signal at ~1670 cm $^{-1}$). Homochiral tripeptides **I** displayed a signal for disordered random coils (Fig. 2A, maximum at 1641 cm^{-1}) and lack of ThT fluorescence (not shown). In contrast, FT-IR confirmed an extended antiparallel beta-sheet conformation (1637 cm^{-1} and 1680-1690 cm^{-1}) for tripeptide enantiomers **II** (i.e., ^{D}Phe-Phe-Val and Phe-^{D}Phe-^{D}Val, Fig. 2B), as suggested by CD. Both peptides self-assemble into elongated fibers, which fluoresce when bound to the amyloid dye (Fig. 3A). Tripeptides **III**, with a central amino acid of different chirality (i.e., Phe-^{D}Phe-Val and ^{D}Phe-Phe-^{D}Val, Fig. 2C) do not have a predominant secondary structure, as suggested by their broad CD signal, clearly the sum of unresolved multiple maxima present in close proximity; only rare extended beta-sheets could be seen in globules by ThT fluorescence microscopy (Fig. 3B). Finally, the FT-IR spectra of enantiomers **IV**, with a *C*-terminus of different chirality (i.e., Phe-Phe-^{D}Val and ^{D}Phe-^{D}Phe-Val, Fig. 2D) also displayed various maxima, highlighting the presence of mixtures of conformers, analogously to enantiomers **III**. In this case, ThT (Fig. 3C) revealed a few aggregates of fluorescent globules, and, occasionally, a few dim needle crystals were seen for Phe-Phe-^{D}Val. In conclusion, from an intermolecular point of view, while the central amino acid plays a key role in driving the chirality of self-assemblies, only tripeptides with the *N*-terminal amino acid of different chirality in their sequence have a predominant conformation of extended, antiparallel beta-sheets that self-assemble in a network of fibrils at physiological pH.

Nanostructure morphology.

Tripeptide self-assembly was also assessed by cryo-TEM (Fig. 4 and ESI) and AFM (Fig. 5 and page S17 in the ESI), recently recognized as an informative technique to monitor fibrillization.[37, 38] In agreement with the above, no ordered nanostructure was observed for the homochiral enantiomers Phe-Phe-Val and ^{D}Phe-^{D}Phe-^{D}Val (see ESI). In contrast, a network of twisted fibers was confirmed by cryo-TEM (Fig. 4A) and AFM (Fig. 5A and ESI) for enantiomers **II**, i.e. ^{D}Phe-Phe-Val and Phe-^{D}Phe-^{D}Val. In agreement with ThT fluorescence images, a few globules and aggregates were revealed by cryoTEM (Fig. 4B-C) and AFM (Fig. 5B-C) for the other stereoisomers, and also a few crystal needles were occasionally seen for ^{D}Phe-^{D}Phe-Val (Fig.

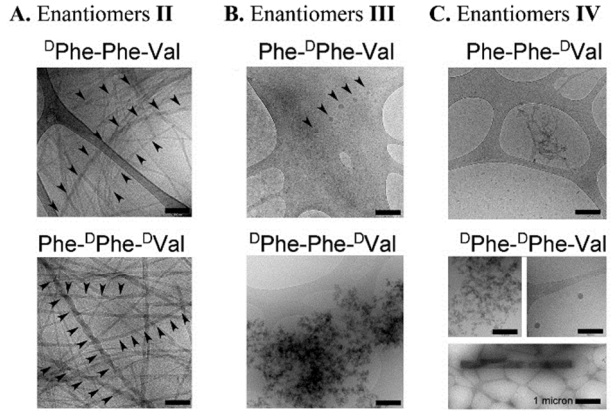

Fig. 4. Cryo-TEM images reveal nanostructures for six tripeptides. Enantiomers **II** (A) are the only ones that self-assemble in a network of fibers that extend over several microns in length; in contrast, isolated structures are seen for enantiomers **III** (B) and **IV** (C). Black arrowheads indicate features of interest, i.e. twisted points of fibers in (A) and globules in (B). Scale bar = 200 nm, except for the labeled insert in the bottom right corner, showing a microcrystal.

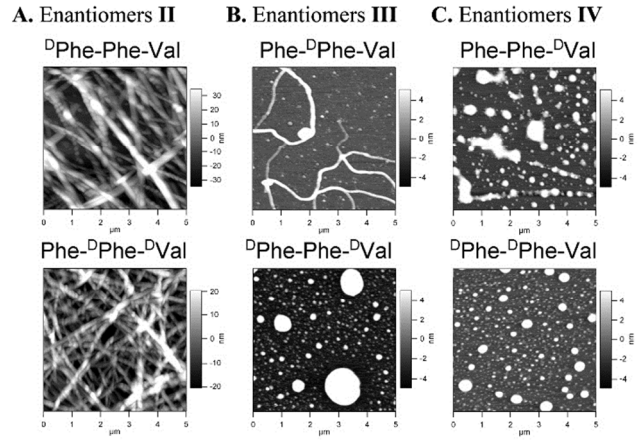

Fig. 5. AFM images reveal nanostructures for six tripeptides.

4C, bottom), which appeared as a highly heterogeneous sample as suggested by its FT-IR spectrum. Interestingly, a few, isolated filaments with globules attached could be seen by cryo-TEM for Phe-Phe-^{D}Val. (Fig. 4C, top), and by AFM for Phe-^{D}Phe-Val (Fig. 5B, top), and the globules observed for Phe-Phe-^{D}Val by AFM appeared at times aligned in a row where coalescence could occur (Fig. 5C, top). This is reminiscent of the early stages of fibril formation as we recently observed for a very similar hydrophobic tripeptide that, under experimental conditions as tested here, nucleates as globules from which short filaments emerge, but do not persist, and are incapable of gelation. In that case, it was sufficient to substitute one L-amino acid with the D-counterpart to achieve the correct molecular shape for the tripeptide to interlock into elongated and persistent fibers, although it was not known how other stereoisomers would behave.[25] The similarity in the spectroscopic profile (e.g., CD, FT-IR, XRD) of the tripeptides from that study and the compounds studied herein suggests that similar mechanisms of fiber self-assembly take place. It is thus tempting to speculate that stereoisomers other than enantiomers **II** (i.e., ^{D}Phe-Phe-Val and Phe-^{D}Phe-^{D}Val) have the tendency towards hydrophobically-driven aggregation; however, nucleated self-assembled structures of such stereoisomers are not stable and ordered enough to rapidly form elongated fibrils. Aggregates of these disordered, hydrophobic tripeptides may then follow different kinetic pathways leading to globules, short filaments, crystals or simply an amorphous precipitate[25] as revealed by our microscopy images.

Rheology

We recently communicated that, following a pH trigger to 7.4, tripeptide ^{D}Phe-Phe-Val self-assembles into a self-supporting hydrogel within a few minutes, however, we did not know the effects of amino acid chirality at other, or multiple, positions of such a short sequence.[24] To answer this question, all its stereoisomers as shown in Table 1 were probed for gelation under the same conditions. All tripeptides have very similar hydrophobicities, as shown by their HPLC retention times (see

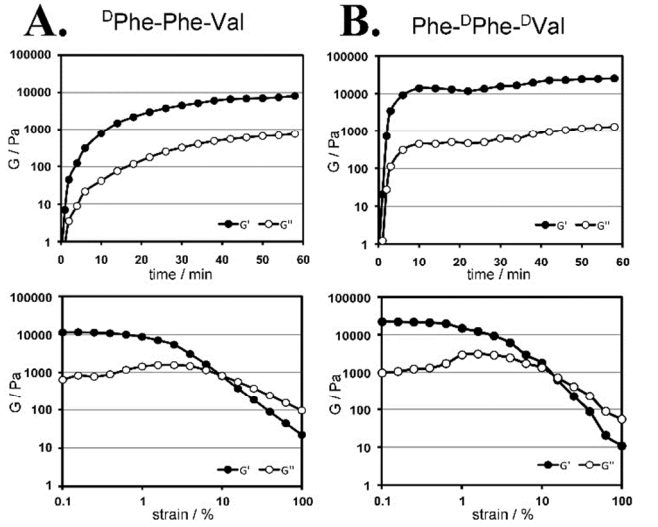

Fig. 6. Rheometric analysis of gelling tripeptides ^{D}Phe-Phe-Val (A) and Phe-^{D}Phe-^{D}Val (B). Elastic (G') and viscous (G") moduli are monitored over time, at a strain of 0.3 % and frequency of 10 rad/s (top), and over strain sweeps at a frequency of 10 rad/s (bottom).

ESI), and limited water solubility. At the concentration tested here, phase separation invariably occurs, resulting in a gel, a precipitate, or needle crystals. The inversion test revealed that only another peptide of the series, i.e. Phe-^{D}Phe-^{D}Val, readily gelates within a few minutes. In contrast, all the other stereoisomers eventually precipitate, and a few needle microcrystals could be observed by eye for ^{D}Phe-^{D}Phe-Val, as supported by the earlier microscopy images. Rheology confirmed these observations, as only noise was recorded for six tripeptides of the series. Interestingly, the only two gelling enantiomers have similar, but not identical, rheological behaviour (Fig. 6 and page S18 in the ESI), as noted also for other gelling enantiomers.[39] Compared to ^{D}Phe-Phe-Val, Phe-^{D}Phe-^{D}Val gelates faster and at any given timepoint achieves a

higher elastic modulus G', for example it reaches 20 kPa within the first hour. Strain and frequency sweeps indicate similar behaviour. Minor differences between these gelling peptides could reflect different fiber density arising from peptide interaction in space with buffer counterions that may assist in the self-assembly process and affect the formation of salt-bridges.

X-Ray Diffraction (XRD) analysis.

XRD was employed to gather a further understanding of the supramolecular arrangement and amyloid nature of the two gelling peptides. Compared to amyloid protein deposits, these biomaterials present weak signals due to the low molecular weight and low concentration of the tripeptides. Thus, we were unable to acquire 2D spectra, and had to rely on 1D XRD analysis (Fig. 7). This revealed reflections corresponding to identical spacings for both enantiomers, although the pattern for Phe-^{D}Phe-^{D}Val is generally more intense, particularly at lower theta, in agreement with higher supramolecular order as suggested by the rheometric analyses discussed above. Amyloid signals were visible (red stars in Fig. 7).[25, 40] The signals at 3.8 Å

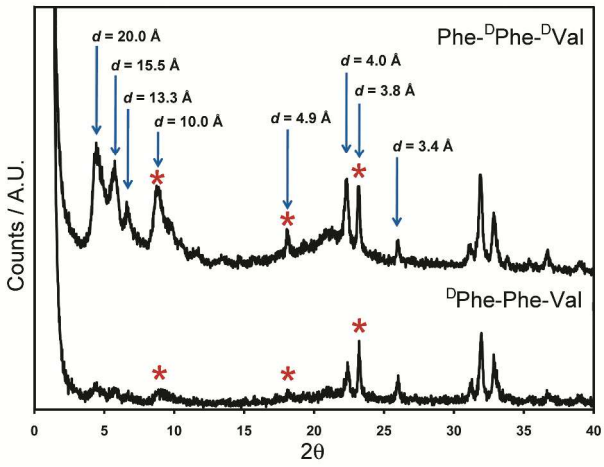

Fig. 7. XRD spectra of gelling tripeptides Phe-^{D}Phe-^{D}Val (top) and ^{D}Phe-Phe-Val (bottom). Red stars denote typical reflections for amyloids with cross-beta structure

and 4.0 Å are generally attributed to distances between aromatic residues involved in π-π stacking. The signal at 4.9 Å is a typical distance for amyloid inter-beta-strand distances, while the peak at 10.0 Å is generally attributed to either the distance between anti-parallel strands (i.e. every other strand) or to inter-sheet distances. A longer spacing of 20.0 Å was also identified, with up to 10 possible reflections, indicative of high supramolecular order and stacking of multiple fibers along the long axis, as seen by cryo-TEM and AFM. Finally, the peak at 3.4 Å is compatible with distances between α-carbons, as seen for similar amyloids.[40]

Cytotoxicity and cell assays

The tripeptide hydrogels described here are intended for biomaterial applications. They were tested for mammalian cell viability using fibroblasts in culture for up to three days. In particular, we were interested to know whether the hydrogels would maintain physical integrity in cell culture conditions, and whether cells would remain viable, adhere to the gels, and/or proliferate. Both gels persisted for the duration of the experiment (Fig. 8), although after three days in culture, microscopy observation revealed instances of fractures within the gel mass (see page S23 of ESI), a sign that gels were starting to lose integrity, likely due to degradation and/or dissolution. Over the time course of the experiment, high cell viability and proliferation were evident and appeared to occur to the same extent in both gels relative to the control (Fig. 8 and pages S18-S23 of ESI). However, cell visualization and quantification in the gels was particularly challenging especially at day 3 when high cell numbers were present in the gels at different focal planes, and we were unable to get high-resolution images of cytoskeletal structure, or to quantify cell viability within the gels via colorimetric assays. Nonetheless, cell penetration and spreading was visible to some extent in both gels, especially at later time points. During the first 24h, cells were located mainly on the top surface of the gels and maintained a spherical morphology, suggesting little or no interaction with the material. At later time points, cells penetrated into the gels and emerging filopodia and spindle-shaped cells could be observed, although cells in the 3D gels never spread to the same extent as on the 2D surface of the plastic control, i.e. the well surface without gel (Fig. 9 and ESI).

We were also particularly interested in whether cells would respond to the differences in chirality between the two enantiomers. Despite the presence of a D-amino acid in a sequence as short as three, ^{D}Phe-Phe-Val maintains a beta-sheet conformation analogous to natural peptides as shown by CD, while its mirror image has the opposite signal as expected for a D-peptide. To our knowledge, this is the first report that directly compares cell viability in gels made of two tripeptide enantiomers, each composed of both D and L amino acids but with conformations of distinct chirality.

In terms of cell viability, we did not observe any significant difference between the two gels, as discussed above. Interestingly, at the 72h timepoint, cell density and viability in both gels was particularly high within the gel mass as opposed to the areas where gel fractures exposed the plastic surface underneath. This suggests fibroblasts' preferential retention in the biomaterial and a non-toxic effect of the dissolved tripeptide, as confirmed by the cytotoxicity assay in solution performed in accordance with ISO 10993 (see page S24 in the ESI). In addition, in the Phe-^{D}Phe-^{D}Val gel, despite it having unnatural beta-sheet chirality, there seemed to be a higher frequency of spreading cells. At present, we cannot rationalize this observation and detail whether there is a predominant cellular

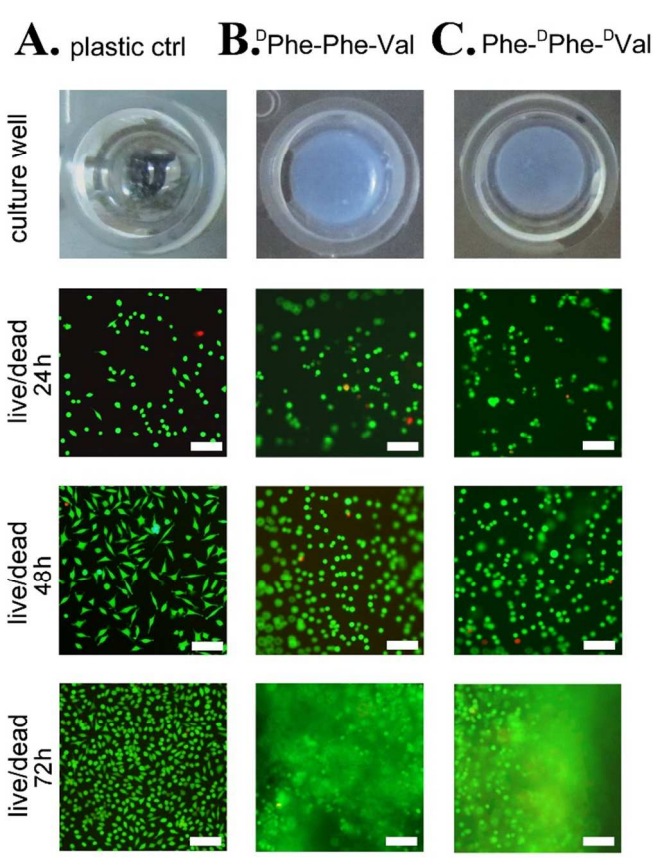

Fig. 8. Images of culture wells and live/dead assays over the course of 72h of fibroblasts grown on plastic control (A) and the two gelling peptides (B, C). Out of focus fluorescence is due to cells on different planes. Scale bar = 100 microns.

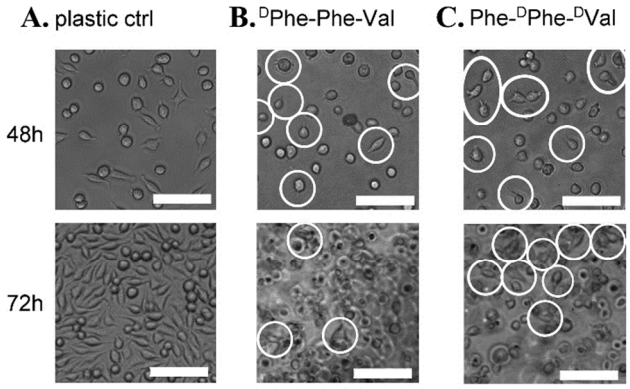

Fig 9. Bright field microscopy images of fibroblast cells cultured on plastic control (A) and the two gelling peptides (B, C). Instances of emerging filopodia and spindle-shaped cells occurred in both gels (white circles).

response to differences in the chemical or rheological properties of the two biomaterials, although both likely play a role. For instance, cell spreading may be a consequence of a mechanical effect, since our rheological analysis shows that at any given timepoint, the Phe-^{D}Phe-^{D}Val gel is stiffer compared to its enantiomer. In addition, the presence of at least one D-amino acid in each peptide bond of this compound will likely slow down its degradation rate by cellular proteases, compared to the enantiomer ^{D}Phe-Phe-Val, which displays one L-peptide bond, leading to an even greater disparity between their respective stiffness. Physical observation of the gels appeared to support this hypothesis, since the Phe-^{D}Phe-^{D}Val gel overall displayed higher mechanical integrity over the three days. In addition, no chiral effects exerted by either peptide in solution on cell adhesion was observed in the cytotoxic assay, with no significant difference in spreading cell numbers between samples, or either sample and control (see page S24 in the ESI). However, chiral effects exerted by supramolecular fibers on cell adhesion cannot be excluded, and would deserve a separate investigation.

Importantly, these results illustrate that peptide gels with unnatural chirality at supramolecular level (i.e. made by Phe-^{D}Phe-^{D}Val) can perform at least as well as their mirror images in cell culture viability, and outperform them in integrity. In addition, cells are able to penetrate into the gels over time and spreading starts to occur. These preliminary results warrant further investigation to better understand heterochiral peptide effects on cellular pathways, as well as the ability of proteases to degrade these biomaterials.

Methods

Peptide synthesis and characterisation

Tripeptides were synthesized and purified using standard Fmoc solid phase peptide synthesis with HBTU activation, following the same procedure described previously, employing reverse-phase HPLC (Agilent Technologies).[24] The HPLC was equipped with a preparative gradient pump (1100/1200), a preparative C-18 column (Luna, 10 microns, 100 Å, 150 x 21.20 mm, Phenomenex), an autosampler (G2260), and a diode array detector (G1365D). The gradient used consisted of acetonitrile (AcN)–water with 0.1% TFA with the following program (10 ml/min flow): t = 0–3 min, 25%AcN; t = 15 min, 55% AcN; t = 16–20 min, 95% AcN.[24] Compounds were freeze-dried; their purity verified by HPLC with the same equipment and gradient as above, but on an analytical C-18 column (Luna, 5 microns, 100 Å, 150 x 4.60 mm, Phenomenex; gradient 5-95% AcN over 15 min.; 1 ml/min flow; t_R= 10-11 min, see ESI). Peptide identity was confirmed by ES-MS, ^{1}H-NMR and ^{13}C-NMR (see ESI).

Peptide gelation

Typically, 4.2 mg of peptide were added to 300 µl of 0.1 M sodium phosphate buffer pH 11.8 and dissolved with the aid of sonication for 5 min in a water bath at room temperature, then diluted 1:1 with another 300 µl of 0.1 M sodium phosphate buffer pH 5.6-5.7 to yield a final pH of 7.4. Samples were sonicated for another 5 min, unless this was not possible due to technical requirements of specific analyses as indicated in the text of each method section. Tripeptides capable of gelation formed a self-supporting hydrogel within minutes, and the second round of sonication simply accelerated the process without affecting the supramolecular structure.[24] All buffer solutions were filtered (0.2 µm) prior to use.

Atomic Force Microscopy (AFM)

An Asylum Research MFP-3D atomic force microscope (Santa Barbara, CA, USA) was used to measure surface topography in tapping mode with ultrasharp silicon nitride tips (NSC15 noncontact silicon cantilevers, MikroMasch, Spain). The tips used in this study had a typical force constant of 40 N/m and a resonant frequency of 320 kHz. Typical scan settings involved the use of an applied piezo deflection voltage of 0.6 – 0.7 V at a scan rate of 0.7 Hz. All images were processed (1st order flattening algorithm) and linescans generated using Igor Pro software. Samples were prepared in a glass vial as described above for the hydrogelation tests and a small amount (~30 µl) was spread onto a clean square of silicon wafer (1 cm x 1 cm) by gently pressing a glass coverslip on top. Samples were then dried in a vacuum oven at room temperature for 24 h.

Cryo-Transmission Electron Microscopy (Cryo-TEM)

A laboratory-built humidity-controlled vitrification system was used to prepare the hydrogels for imaging in a thin layer of vitrified ice using cryo-TEM. Humidity was kept close to 80 % for all experiments, and ambient temperature was 22°C. 200-mesh copper grids coated with perforated carbon film (Lacey carbon film: ProSciTech, Qld, Australia) were used for all experiments. Grids were glow discharged in nitrogen for 5 seconds immediately before use. Hydrogels were prepared as described above. At time of analysis, hydrogels were disrupted by tapping against the glass vial, and samples were agitated with the pipette tip according to a well-established protocol for high viscosity systems.[41] Approximately 4 µL aliquots of sample were pipetted onto each grid prior to plunging. In the case of samples which could not be liquefied adequately, the gel was smeared gently onto the grid. After 30 seconds adsorption time the grid was blotted manually using Whatman 541 filter paper, for approximately 6-10 seconds. Blotting time was optimised for each sample. The grid was then plunged into liquid ethane cooled by liquid nitrogen. Frozen grids were stored in liquid nitrogen until required. The samples were examined using a Gatan 626 cryoholder (Gatan, Pleasanton, CA, USA) and Tecnai 12 TEM (FEI, Eindhoven, The Netherlands) at an operating voltage of 120 kV. At all times low dose procedures were followed, using an electron dose of 8-10 electrons/Å^2 for all imaging. Images were recorded using either a Megaview III CCD camera and AnalySIS camera control software (Olympus.) using magnifications in the range 40 000x to 110 000x, or a FEI Eagle 4k x 4k CCD camera (FEI, Eindhoven, The Netherlands) at magnifications in the range 15,000 – 30,000x.

Circular Dichroism Spectroscopy (CD)

The secondary structure of peptides was analysed using a 0.1 cm quartz cell on a Jasco J815 Spectropolarimeter, with 1 s integrations and a step size of 1 nm with a bandwidth of 1 nm over a range of wavelengths from 200 to 280 nm. Peptide samples were freshly prepared by mixing the two precursor solutions directly in the CD cell, thus, without the second round of sonication, to preserve the quartz cell. Spectra were recorded after 15 min. Measurements were repeated at least 5 times, and to reduce the noise near 200 nm, their average is plotted.

Fourier-Transformed Infrared Spectroscopy (FT-IR)

FT-IR spectra were collected on a Nicolet 6700 FT-IR spectrometer in ATR mode. A portion of the gel was transferred onto a clean piece of silicon wafer (1 cm x 1 cm), then gently spread over the surface by pressing a coverslip on top; the coverslip was immediately removed and samples dried under vacuum for 24h. Dried samples on the silicon wafers were placed directly onto the ATR crystal. Scans were between 1800 and 1500 cm^{-1} with 80 accumulations at a resolution of 0.4 cm^{-1}.

Rheometry

Dynamic time sweep rheological analysis was conducted on an Ares rheometer (TA Instruments, USA) with a 25 mm aluminium parallel plate geometry. A Peltier temperature controller was connected to the rheometer to maintain a temperature of 25 °C. Peptide samples were freshly prepared by mixing the two precursor solutions directly on the rheometer to register early stages of gelation, thus without the second round of sonication. Samples were immediately analysed with a gap of 300 µm, strain of 0.3 % and frequency of 10 rad/s. After 60 minutes of gelation, strain sweeps were recorded with a frequency of 10 rad/s and frequency sweeps with strain of 0.3%. Data acquisition was repeated in triplicates, and average values plotted.

Thioflavin T (ThT) confocal fluorescence microscopy

Gel precursor solutions were prepared as indicated above and 12.5 µl of each were immediately placed on wells of a "µ-Slide Angiogenesis" uncoated (Ibidi, Germany, through DKSH Australia). 25 µl of a solution of ThT (200 µM in 50 mM Glycine-NaOH pH 7.5, 0.2 µm-filtered) were placed on top. After 15 minutes, the slides were imaged on a Leica SP5 microscope (63x water immersion objective, NA 1.2, ex. 458 nm, em. 468-600 nm). Samples treated and stained with an identical protocol but without the peptide, were used as control and did not reveal any of the fluorescent structures described in the text (data not shown).

X-Ray fiber Diffraction (XRD)

A Bruker D8 Advance X-ray Diffractometer with CuK α radiation (40 kV, 40 mA) equipped with a LynxEye silicon strip detector was employed to determine the X-ray diffraction (XRD) patterns. Each sample was scanned over the 2-theta range from 1º to 60° with a step size of 0.02° and a count time of 1.6 seconds per step. An air scatter slit was used to reduce the beam intensity at low angles. Analyses were performed on the collected XRD data for each sample using the Bruker XRD search match program EVA™. Samples were mounted on zero background plates consisting of a silicon wafer located in a standard Bruker specimen holder, and were dried overnight in air.

Cell assays

Tripeptides in solution were assessed for cytotoxicity in accordance with ISO 10993, and tripeptide gels were also probed for their ability to support cell viability and proliferation. For cytotoxicity studies, L929 mouse fibroblast cells were seeded at 10000 cells/well of a 96-well tissue culture plate in 100 µl of media (MEM + GlutaMAX^{TM}-I (GIBCO), supplemented with 1 v% NEAA (non-essential amino acids, GIBCO), 2 v% Anti-Anti (Antimycotic-Antibiotic, GIBCO), and 10 v% FBS (fetal bovine serum, SAFC Biosciences) and cultured at 37 °C, 5 % CO_2 overnight. Tripeptides were dissolved in the media at the highest concentration possible without occurrence of precipitation or gelation (i.e., 1 mg/ml) and 1:1 serial dilutions down to < 8 µg/ml were prepared. The tripeptide solutions were sterile-filtered and 100 µl were applied to monolayers that were then cultured a further 24 hours. Cells were imaged on an inverted microscope (Olympus IX71) before quantitation by reduction of resazurin (120 µl of a 1:9 solution of PrestoBlue® in media for 1.5 hours) and 100 µl assayed for fluorescence on a Pherastar fluorometer (ex.540-20 nm, em. 590-20 nm). Media without tripeptide as negative control, and 5 v% dimethylsulphoxide (DMSO) in media as positive control, were included. Monolayers remained subconfluent throughout. For gel studies, gel precursor solutions were prepared as indicated previously and 15 µl of each were mixed directly in triplicate wells of a "µ-Slide Angiogenesis" uncoated (Ibidi, Germany, through DKSH Australia), thus without the second round of sonication. After 24 h, gels were pre-treated with 30 µl of media for 1 h. L929s were added to the gels (10 000 cells/cm2 in 30 µl media), and cultured at 37 °C, 5 % CO_2 for up to 72 h, by handling the slides according to the manufacturers' instructions, including the addition a few drops of deionised water in the empty space between the wells to minimise sample evaporation. Every 24 h, cells were either stained for viability or, if continuing to a later assay time point, had 30 µl of media exchanged for fresh media. Cell viability was investigated using the LIVE/DEAD® assay (Invitrogen), according to the manufacturers' instructions. Cells were imaged on an inverted microscope (Nikon Eclipse TE2000-U) for Calcein (ex. 465-495 nm, em. 515-555 nm) and ethidium (ex. 510-560 nm, em. > 590 nm).

Conclusions

This work shows how subtle changes in chirality at each position along a tripeptide sequence have a profound impact on conformation and supramolecular behaviour of uncapped tripeptides (Scheme 1). Importantly, our data highlights how the chirality of the central amino acid relative to the rest of the sequence of three is a key element in driving the chirality of intermolecular interactions as observed by CD, although on its own it is not sufficient to drive self-assembly into a macroscopic hydrogel. In fact, 3D molecular shape and steric hindrance are known to be key features for peptide interlocking into persistent self-assembled structures; in addition, terminal phenylalanine residues also play a role, with the establishment of Phe zippers.[25] Self-assembling tripeptide isomers selectively organise into anti-parallel beta-sheets, and establish a number of non-covalent interactions, i.e. Phe π-π stacking, hydrogen bonding between amides of the peptide backbone, and extended salt bridges between the zwitterion termini.[24]

Here we show that only the two Phe-Phe-Val stereoisomers with the *N*-terminal of different chirality to the rest of the sequence gel at physiological pH. The importance of the *N*-terminal residue can be envisaged in light of the fact that these systems exploit a pH switch from alkaline (above the terminal amine pKa) to neutral (below its pKa), thus a change in the *N*-terminal (but not *C*-terminal) protonation state is expected. This observation also applies to ^{D}Leu-Phe-Phe[25] and ^{D}Val-Phe-Phe[24], which are pH-triggered hydrogelators similar to ^{D}Phe-PheVal. In addition, no hydrogel was observed for any of their L-homochiral counterparts. However, as this work shows instances of limited self-assembly, but no gelation, for other Phe-Phe-Val heterochiral peptides, we cannot exclude that similar hydrophobic, heterochiral sequences may have more appropriate steric features to drive further self-assembly and form a hydrogel. Thus, while we can envisage similar self-assembling behaviour will apply to other hydrophobic tripeptides containing the Phe-Phe motif, each sequence will have different steric properties and should be separately evaluated.

Importantly, the two gelling enantiomers ^{D}Phe-Phe-Val and Phe-^{D}Phe-^{D}Val equally support high viability and proliferation of mammalian cells *in vitro*, while in solution they do not elicit a cytotoxic response. Interestingly, despite one peptide having unnatural beta-sheet chirality as seen by CD, cells still penetrate and slowly spread in this biomaterial over time. This study raises interesting questions as to how cells sense and interact with peptide chirality, but especially shows that while homochirality is nature's choice, heterochiral tripeptides may be viable biomaterials and offer new cost-effective tools to answer unresolved questions in biology.

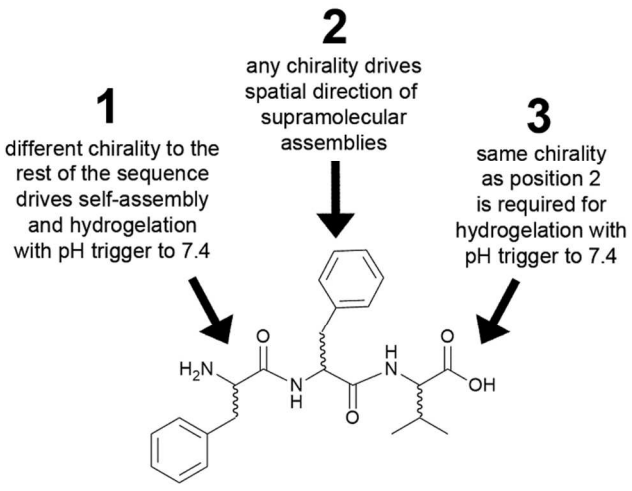

Scheme 1. Effects of chirality at each amino acid position of Phe-Phe-Val tripeptides on self-assembly and hydrogelaton at pH 7.4.

Acknowledgements

The authors acknowledge the CSIRO – Monash University Collaborative Research Support Scheme (CRSS) for funding. The facilities of Monash Micro Imaging, Monash University, Australia, and in particular Stephen Firth, Dr. Judy Callaghan and Dr. Alex Fulcher are also acknowledged for their scientific and technical assistance.

Notes and references

[a] CSIRO Materials Science and Engineering, Bayview Avenue, Clayton, VIC 3053, Australia.

[b] Present address: INSTM, University of Trieste, Via L. Giorgieri 1, 34127 Trieste, Italy. email: marchesan.silvia@gmail.com

[c] La Trobe University, Department of Chemistry, La Trobe Institute of Molecular Sciences, Kingsbury Drive, Bundoora, Melbourne VIC 3086, Australia.

[d] Department of Materials Engineering, Monash University, Victoria 3800, Australia.

Electronic Supplementary Information (ESI) available: spectroscopic peptide characterisation data (^{1}H and ^{13}C NMR, ES-MS, HPLC), additional rheometric data, microscopy images and cytotoxicity assay data. See DOI: 10.1039/b000000x/

1. A. Dasgupta, J. H. Mondal and D. Das, *RSC Adv.*, 2013, **3**, 9117-9149.
2. H. M. Wang and Z. M. Yang, *Nanoscale*, 2012, **4**, 5259-5267.
3. H. M. Wang, Z. M. Yang and D. J. Adams, *Mater. Today*, 2012, **15**, 500-507.
4. E. Busseron, Y. Ruff, E. Moulin and N. Giuseppone, *Nanoscale*, 2013, **5**, 7098-7140.
5. T.-Y. Cheng, H.-C. Wu, M.-Y. Huang, W.-H. Chang, C.-H. Lee and T.-W. Wang, *Nanoscale*, 2013, **5**, 2734-2744.
6. D. Silva, A. Natalello, B. Sanii, R. Vasita, G. Saracino, R. N. Zuckermann, S. M. Doglia and F. Gelain, *Nanoscale*, 2013, **5**, 704-718.
7. J. Raeburn, A. Z. Cardoso and D. J. Adams, *Chemical Society Reviews*, 2013, **42**, 5143-5156.
8. W. Li, Y. Kim and M. Lee, *Nanoscale*, 2013, **5**, 7711-7723.
9. Y. Liu, Y. Yang, C. Wang and X. Zhao, *Nanoscale*, 2013, **5**, 6413-6421.
10. M. D. Segarra-Maset, V. J. Nebot, J. F. Miravet and B. Escuder, *Chem. Soc. Rev.*, 2013, **42**, 7086-7098.
11. C. J. Bowerman and B. L. Nilsson, *J. Am. Chem. Soc.*, 2010, **132**, 9526-9527.
12. L. Chen, T. O. McDonald and D. J. Adams, *RSC Adv.*, 2013, **3**, 8714-8720.
13. P. N. Cheng, J. D. Pham and J. S. Nowick, *J. Am. Chem. Soc.*, 2013, **135**, 5477-5492.
14. C. X. Wang, A. H. Yang, X. Li, D. H. Li, M. Zhang, H. W. Du, C. Li, Y. Y. Guo, X. B. Mao, M. D. Dong, F. Besenbacher, Y. L. Yang and C. Wang, *Nanoscale*, 2012, **4**, 1895-1909.
15. S. H. Kim and J. R. Parquette, *Nanoscale*, 2012, **4**, 6940-6947.
16. A. Dehsorkhi, I. W. Hamley, J. Seitsonen and J. Ruokolainen, *Langmuir*, 2013, **29**, 6665-6672.
17. D. J. Adams, *Macromol. Biosci.*, 2011, **11**, 160-173.
18. J. E. Gough, A. Saiani and A. F. Miller, in *Bioinspired, Biomimetic and Nanobiomaterials*, 2012, vol. 1, pp. 4-12.
19. M. Zhou, A. M. Smith, A. K. Das, N. W. Hodson, R. F. Collins, R. V. Ulijn and J. E. Gough, *Biomaterials*, 2009, **30**, 2523-2530.
20. T. Liebmann, S. Rydholm, V. Akpe and H. Brismar, *BMC biotechnology*, 2007, **7**, 88.
21. B. Ding, Y. Li, M. Qin, Y. Ding, Y. Cao and W. Wang, *Soft Matter*, 2013, **9**, 4672-4680.
22. J. Raeburn, T. O. McDonald and D. J. Adams, *Chem. Commun.*, 2012, **48**, 9355-9357.
23. D. J. Adams, M. F. Butler, W. J. Frith, M. Kirkland, L. Mullen and P. Sanderson, *Soft Matter*, 2009, **5**, 1856-1862.
24. S. Marchesan, C. D. Easton, F. Kushkaki, L. Waddington and P. G. Hartley, *Chem Commun*, 2012, **48**, 2195-2197.
25. S. Marchesan, L. Waddington, C. D. Easton, D. A. Winkler, L. Goodall, J. Forsythe and P. G. Hartley, *Nanoscale*, 2012, **4**, 6752-6760.
26. S. Marchesan, Y. Qu, L. J. Waddington, C. D. Easton, V. Glattauer, T. J. Lithgow, K. M. McLean, J. S. Forsythe and P. G. Hartley, *Biomaterials*, 2013, **34**, 3678-3687.
27. S. Marchesan, L. Waddington, C. Easton, F. Kushkaki, K. McLean, J. Forsythe and P. Hartley, *BioNanoSci.*, 2013, **3**, 21-29.
28. P. Ung and D. A. Winkler, *J. Med. Chem.*, 2011, **54**, 1111-1125.
29. M. X. Zhang, G. Y. Qing and T. L. Sun, *Chem. Soc. Rev.*, 2012, **41**, 1972-1984.
30. M. B. Taraban, Y. Feng, B. Hammouda, L. L. Hyland and Y. B. Yu, *Chem. Mater.*, 2012, **24**, 2299-2310.
31. L. L. Hyland, J. D. Twomey, S. Vogel, A. H. Hsieh and Y. B. Yu, *Biomacromol.*, 2013, **14**, 406-412.
32. M. C. Branco, D. J. Pochan, N. J. Wagner and J. P. Schneider, *Biomaterials*, 2009, **30**, 1339-1347.
33. Z. Luo and S. Zhang, *Chem. Soc. Rev.*, 2013, **41**, 4736-4754.
34. J. Li, Y. Gao, Y. Kuang, J. Shi, X. Du, J. Zhou, H. Wang, Z. Yang and B. Xu, *J. Am. Chem. Soc.*, 2013, **135**, 9907-9914.
35. Y. Fu, B. Li, Z. Huang, Y. Li and Y. Yang, *Langmuir*, 2013, **29**, 6013-6017.
36. J. E. Shea, C. Wu, M. Biancalana and S. Koide, *J. Mol. Biol.*, 2009, **394**, 627-633.
37. J. Adamcik, J. M. Jung, J. Flakowski, P. De Los Rios, G. Dietler and R. Mezzenga, *Nat. Nanotechnol.*, 2010, **5**, 423-428.
38. J. Adamcik and R. Mezzenga, *Curr. Opin. Colloid Interface Sci.*, 2012, **17**, 369-376.
39. Z. Luo, S. Wang and S. Zhang, *Biomaterials*, 2011, **32**, 2013-2020.
40. B. Ma and R. Nussinov, *Proc. Natl. Acad. Sci. U. S. A.*, 2002, **99**, 14126-14131.
41. T. Yeshayahu, in *Giant Micelles*, CRC Press, 2007, pp. 163-178.